# A Novel Overlapping ME Peaks Decomposition Algorithm Based on Iterative Derivative Sharpening

Wenhe He, Hui You, Zihao Lu, Yaping Liu, Yuanfen Chen, Ying Liu, and Cuimin Sun

***Abstract*— In microchip electrophoresis (ME) signals, multiple subpeaks low-resolution overlapping peaks seriously interfere with the measurement of peak parameters. However, the existing peak analysis methods either address the problem of two subpeaks overlapping peaks or set peak parameters empirically. In this study, an automatic overlapping peaks decomposition algorithm based on signal smoothing, iterative sharpening, and peak fitting is proposed. First, the Savitzky–Golay (SG) filter is used for smoothing ME signals because it outperforms other smoothing methods in peak retention ability, smoothness, and preservation of the high-frequency information content of the signal. Second, an iterative peak sharpening strategy is proposed based on the principle of the even-order derivative method. Finally, overlapping peak analysis methods based on swarm intelligence algorithms, gradient algorithms, and simplex algorithms, respectively, are proposed. For the swarm intelligence-based fitting algorithms, the fitting errors (fes) of ME signals using the proposed peak sharpening strategy are reduced by 13.5%, 23.7%, and 40.0% on average, respectively.**

***Index Terms*— Even-order derivative sharpening, microchip electrophoresis (ME), overlapping peaks decomposition, peak fitting, Savitzky–Golay (SG) filter.**

## NOMENCLATURE

| | |
|---|---|
| ME | Microchip electrophoresis. |
| SLSMA | Sigmoidal membership function and Lévy flight-based slime mold algorithm. |
| TWOA | Tent map-based whale optimization algorithm. |
| PSO | Particle swarm optimization. |
| LM | Levenberg–Marquardt. |
| TRR | Trust region reflective. |
| NM | Nelder–Mead. |
| SG | Savitzky–Golay. |
| Wl | Wavelet. |
| Bw | Butterworth. |
| Et | Elliptic. |
| sc | Sharpening coefficient. |
| fe | Fitting error. |
| Los | Length of signal. |
| grfe | Growth rate of fe. |
| Th | Threshold. |
| SNR | Signal-to-noise ratio. |
| CI | Chebyshev I. |
| CII | Chebyshev II. |

Manuscript received 20 October 2023; revised 16 January 2024; accepted 29 January 2024. Date of publication 7 March 2024; date of current version 19 March 2024. This work was supported in part by the National Natural Science Foundation of China under Grant 62304057, in part by Guangxi Bagui Scholars Project under Grant 2019A02, in part by the Science and Technology Major Project of Guangxi under Grant AA22117005 and Grant AA22117007, and in part by Guangxi University Innovation and Development Multiplication Program Project under Grant 202201343 and Grant 202201369. The Associate Editor coordinating the review process was Dr. Shiwu Zhang. *(Corresponding author: Cuimin Sun.)*

Wenhe He is with the School of Electrical Engineering, Guangxi University, Nanning 530004, China (e-mail: 1812401002@st.gxu.edu.cn).

Hui You, Zihao Lu, Yaping Liu, and Yuanfen Chen are with the School of Mechanical Engineering, Guangxi University, Nanning 530004, China (e-mail: usmlhy@iim.ac.cn; 17862722921@163.com; 2011391061@st.gxu.edu.cn; yuanfenchen@gxu.edu.cn).

Ying Liu is with the School of Civil Engineering and Architecture, Guangxi University, Nanning 530004, China (e-mail: lyily1112@126.com).

Cuimin Sun is with the School of Computer, Electronics and Information, Guangxi University, Nanning 530004, China (e-mail: cmsun@gxu.edu.cn).

Digital Object Identifier 10.1109/TIM.2024.3374307

## I. INTRODUCTION

RECENTLY, ME has been considered as a promising detection technique that is gaining increasing attention. The detection results of exosomes [1] and heavy metals [2] samples show the wide application of ME. However, the overlapping peaks problem [3], [4], [5], [6] is a serious challenge for ME signal analysis. Thus, to accurately measure component peaks (cps) in ME signals, further research is needed on the analysis of low-resolution overlapping peaks.

In the last five years, the analysis methods of peak-shaped signals based on optimization algorithms have been proposed. These methods can be classified into three categories, namely, swarm intelligence algorithms [7], [8], [9], gradient algorithms [10], [11], and simplex algorithms [12]. Specifically, the SLSMA [7] and the TWOA [8] were used for the fitting analysis of overlapping ME peaks by exploiting the global optimization capability of the swarm intelligence algorithm. Furthermore, the PSO algorithm [9] based peak detection method for chewing signals analysis also extends the application of swarm intelligence algorithms. For the gradient algorithms, the LM algorithm [10] and the TRR algorithm [11] were used for the fitting analysis of the measured spectra of methane and the gamma-ray spectroscopy peaks, respectively. In addition, the application of the NM [12] algorithm to mass spectrometry peak analysis demonstrates the optimization capability of the simplex algorithm. These three types of algorithms are more accurate for the analysis of overlapping peaks with higher resolution. However, for noisy multiple

subpeaks low-resolution overlapping peaks in complex ME signals, these algorithms may obtain lower fitting accuracy if the initial fitting parameters are not set appropriately.

For low-resolution overlapping peak problems, related studies have focused on resolution enhancement methods. In 2016, Li et al. [13] proposed a signal enhancement method to analyze overlapping peaks consisting of the Gaussian and Lorentzian peaks. This study investigated the range of scs and was applied to the analysis of mass spectrometry signals. In 2019, to increase the resolution of the detected signal, Wahab et al. [14] proposed a derivative enhancement method. The effectiveness of this method was tested by trailing and shoulder peaks. Furthermore, by empirically setting the sc, this method was applied to the analysis of chromatographic overlapping peaks. To increase the resolution of double Gaussian overlapping peaks, Chen et al. [15] proposed a signal enhancement method based on second-order derivatives. This method can adaptively enhance the signal and is effective for the analysis of mass spectrometry signals with double subpeaks overlapping. In 2020, to rapidly increase the peak capacity, Hellinghausen et al. [16] used the even-order derivative method to enhance the resolution of ultrahigh-pressure liquid chromatography. In 2021, Sun and Xin [17] derived an upper bound for the sc applicable to the Lorentzian overlapping peaks. This second-order derivative method was used to sharpen the nuclear magnetic resonance spectroscopy. In 2022, the even-order derivative method [18] was used to enhance the resolution of the pulse-coherent Doppler wind LiDAR signals by empirically setting the sc. These studies explored the application of the even-order derivative method in enhancing the resolution of overlapping peaks. However, these methods either target the case where only two subpeaks overlap [15] or the sc is set empirically [13], [14], [18], making it difficult to apply directly to the multiple subpeaks overlapping peaks problem in ME signals.

It is worth noting that signal enhancement methods based on even-order derivatives are sensitive to noise, so the choice of signal smoothing method is also important. For example, the SG filter was used for smoothing mass spectral signals [15]. Sadeghi et al. [19] analyzed the optimal window length for different orders of SG filter. This method was used for noisy signal recovery. Hasan et al. [20] showed that SG filter can remove harmonics and does not cause distortion of grid voltage signal. In addition to the SG filter, commonly used signal smoothing methods include Wl denoising [21], Bw filter [22], Chebyshev filter [23], and Et filter [24]. It can be seen that these methods have been widely used in the smoothing of different kinds of signals. There are few studies on the smoothing of ME signals. Moreover, to analyze ME signals, the smoothing method should be able to maintain the peak positions.

From the above literature review, the following gaps exist in the existing peak analysis methods.

1) Initialization of fitting parameters using manual setting of the number of peaks or manual selection of the position of each subpeak.
2) Setting the sc empirically during the resolution enhancement process.
3) Lack of evaluation criteria for signal smoothing methods related to the even-order derivative sharpening method.
4) Fewer types of algorithms are used simultaneously in the fitting process.

To try to mitigate those gaps, an overlapping peak decomposition method based on an iterative sharpening peak-finding strategy is proposed in this work. The differences between the strategy proposed in this article and those published in recent years are as follows: to analyze the fiber Bragg grating signal, the method proposed by Wang et al. [25] requires the Hilbert transform of the signal, while the method proposed by Kumar and Sengupta [26] requires the Wl transform and the great likelihood estimation; the method proposed by Sadat and Joye [27] requires the assistance of peak analysis software such as OriginPro for Fourier transform infrared and Raman spectroscopy; the method proposed by Kalesse et al. [28] needs to manually set up the training set for supervised learning to analyze the radar Doppler spectra. As a key step in this study, the peak finding process combines peak sharpening and sliding window [29] methods. The main contributions of this study are as follows.

1) A strategy combining smoothing, sharpening, and peak localization is proposed to automatically obtain peak fitting parameters.
2) An iterative peak sharpening method is proposed, which updates the scs based on the number of peaks and the fe.
3) Metrics for selecting signal smoothing method are defined to evaluate the peak position retention capability and smoothing.
4) We compared the peak fitting performance of different optimization algorithms using synthetic and ME signals to verify the effectiveness of the proposed sharpening strategy.

The rest of this article is organized as follows. In Section II, the proposed overlapping peak analysis method is described. Section III describes the fitting results of different algorithms for synthetic and ME signals. Discussion and conclusion are given in Sections IV and V, respectively.

## II. Methodology

In this work, a peak decomposition method based on iterative sharpening is proposed. The proposed method consists of three main steps: smoothing, sharpening and localization, and fitting. Next, these major steps will be presented in a step-by-step manner.

### A. Signal Smoothing

Influenced by the performance of the detection instrument, the ME signal cannot avoid the presence of noise, which will interfere with the sharpening and fitting of the peaks. Therefore, smoothing of the noisy signal is the first step of the proposed method, which can be usually achieved by filtering. SG is an effective filtering method that has been used for the smoothing of grid voltage signals [20] and the recovery of noisy signals [19]. Therefore, in the work, the SG is used to smooth the ME signal before sharpening. The SG filter

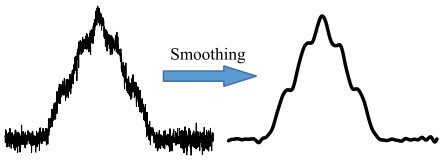


Fig. 1. Illustration of the signal smoothing process.

performs a least-squares polynomial fit to the signal in the window with the following objective function (objf)

$$\text{objf} = \sum_{i=-M}^{M}\left(\sum_{k=0}^{N}\text{cof}_k \times i^k - \text{sf}_i\right)^2 \tag{1}$$

where cof is the polynomial coefficient, $N = 2M + 1$ is the length of the filter window, and sf is the signal to be filtered. It should be noted that the symbol $\times$ represents the multiplication operation.

This filtering process can be considered a convolution operation, and the filtered signal is given as follows:

$$\text{fs}(k) = \sum_{-M}^{M}\text{fir}_i \times \text{sf}_{k-i} = \sum_{-M}^{M}\text{fir}_{k-i} \times \text{sf}_i \tag{2}$$

where fir is the fixed impulse response.

Inspired by Wang et al. [30], we graphically represent each key step to visualize the proposed method. Fig. 1 illustrates the process of signal smoothing. As can be seen from Fig. 1, the original signal on the left contains noise and cannot be sharpened directly using the even-order derivative method. By signal smoothing operation, the signal obtained is smoother and conducive to peak sharpening.

In this study, the peak position retention capability, smoothness, and signal content preservation of those signal smoothing methods are compared. First, the effect of different smoothing methods on the high-frequency information content of the signal can be analyzed by comparing the SNR. Second, the peak positions of the smoothed signal are required to be close to those of the original signal in order to fit the original signal. Third, the smoothed signal should be relatively smooth in order to be sharpened using the even-order derivative method.

The mathematical expression for SNR [31] is as follows:

$$\text{SNR} = 10\log_{10}\frac{\sum_{i=1}^{N}(S1_i)^2}{\sum_{i=1}^{N}(S1_i - S2_i)^2} \tag{3}$$

where $N$ denotes the number of data points in the signal, and $S1$ and $S2$ denote the signal before and after smoothing, respectively.

The peak position retention capability is defined as the horizontal distance between the maxima of the signal, before and after smoothing, as follows:

$$\text{Distance} = |t\text{max}1 - t\text{max}2| \tag{4}$$

where $||$ represents the absolute value operator, $t$max1 and $t$max2 represent the horizontal coordinate values of the maxima of the original and smoothed signals, respectively.

Let both $A$ and $B$ be signal-smoothing methods. Then, the relative smoothness of $A$ with respect to $B$ is defined as follows:

$$\text{Smoothness}(A, B) = \text{std}(S3_B)/\text{std}(S3_A) \tag{5}$$

where std denotes the standard deviation, and $S3$ denotes the first-order derivative of the smoothed signal. Smoothness denotes the degree of fluctuation of the smoothed signal.

It is worth noting that the choice of smoothing method should also be able to remove noise while preserving the information content of the signal. A comparison of different signal smoothing methods will be given in Section III.

After the smoothing of the signal, the overlapping peak decomposition algorithm proposed in this study moves to the peaks sharpening and localization step, which will be discussed in subsection II-B.

### B. Peaks Sharpening and Localization

In the study, the step is followed by peak fitting. For the peaks fitting problem, it is a challenge when lower resolution peaks are present in the smoothed signal. A common mathematical method for improving peak resolution is the even-order derivative [14] method. Visually, this method makes the peaks sharper; hence, it is called the peaks sharpening method. The mathematical expression [18] of the peaks sharpening method is as follows:

$$\text{ss} = s + \sum_{1}^{n}\left((-1)^i \times \text{sc}_i \times s^{(2i)}\right) \tag{6}$$

where ss is the sharpened signal, $s$ is the signal to be sharpened, $n$ is the number of derivatives, sc is the sharpening coefficient, and $s^{(2i)}$ is the derivative of $s$.

From (6), the sharpening process approximates a Taylor expansion. In (6), the value of sc determines the sharpening effect of the signal, which affects the results of peak localization. Therefore, it is important to choose a suitable sc value. The appropriate sc should allow the signal to be moderately sharpened to locate the desired peak position. Theoretically, sc can be any real number. When the sc is too small, it is difficult to locate the desired peaks. On the contrary, false peaks may be localized for too large sc. Thus, the selection of the appropriate sc is important. In existing studies, analysts need to select sc empirically, and these manual methods affect the automatic analysis of the signal. To the best of the authors' knowledge, there are no relevant methods for studying iterative scs for low-resolution multiple subpeaks overlapping peaks, which is the motivation for this article.

In the proposed method, peak sharpening and peak position localization are the key steps. Peak sharpening facilitates peak localization, which is then used to initialize the peak fitting algorithm. To locate each peak position, (6) is used to enhance the peak resolution of the smoothed signal. For ME signals, the horizontal coordinate is the index of the data, and the vertical coordinate is the strength of the signal. Thus, the position of a peak can be represented by its index in the ME signal. In this study, a peak localization procedure that takes the index of the local maximum of the signal within the window as the

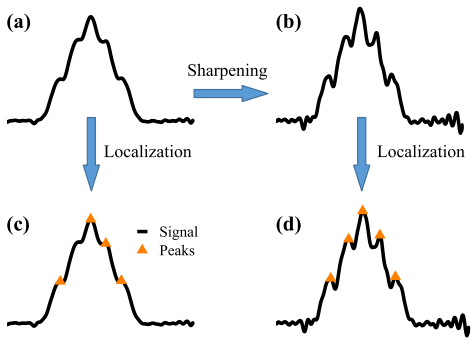


Fig. 2. Illustration of the peak sharpening and localization process. (a) Smoothed signal. (b) Sharpened signal. (c) Result of peak localization of the smoothed signal. (d) Peak localization result of the sharpened signal.

peak position is developed. The mathematical expression of this procedure is shown in the following equation:

$$\mathrm{fp} = \max(\mathrm{ss}(i)), \quad i \in [W\mathrm{min}, W\mathrm{max}] \tag{7}$$

where fp is the position of the peaks found, ss has the same meaning as in (6), $i$ is the index of the signal, and $W$min and $W$max denote the start and end of the peak localization window, respectively. For ease of description, we define the length of fp as the term "found peaks."

Fig. 2 illustrates the process of peak sharpening and localization. From Fig. 2, it can be seen that the number of peaks that can be localized for the sharpened signal is much higher. This will facilitate the fitting analysis of overlapping peaks.

### C. Peaks Fitting

Usually, the ME signal contains the peaks corresponding to the individual components of the sample and the noisy baseline of the system. According to a recently published study [7], the cps can be represented as Gaussian peaks (gps) and the noisy baseline as noise (ns) and baseline (bl). Therefore, the ME signal with $N$ peaks can be expressed as follows:

$$\mathrm{sme}(t) = \mathrm{ns}(t) + \mathrm{bl}(t) + \sum_{1}^{N} \mathrm{cp}_i(t) \tag{8}$$

where sme is the ME signal.

To facilitate the analysis, the baseline correction of the signal is required. In this work, gps are used to fit the ME signal. A unit height gp with position (pos) and width (wid) can be expressed as follows:

$$\mathrm{gp}(t) = e^{-((t-\mathrm{pos})/\mathrm{wid})^2 \times \ln 16}. \tag{9}$$

According to [7], the cps of the ME signal can be fit as the sum of gps, and the fe can be expressed as follows:

$$\mathrm{fe} = \left\| \sum_{i}^{N} (h_i \times \mathrm{gp}_i(t) - \mathrm{cp}_i(t)) \right\|_2 \Big/ \sqrt{\mathrm{Los}} \tag{10}$$

where $h_i$ is the height of the $i$th gp and Los is the length of the signal. To minimize fe, it is necessary to give relatively accurate initial values of peak parameters for the fitting algorithm. In this work, the fp in (7) is used to initialize the

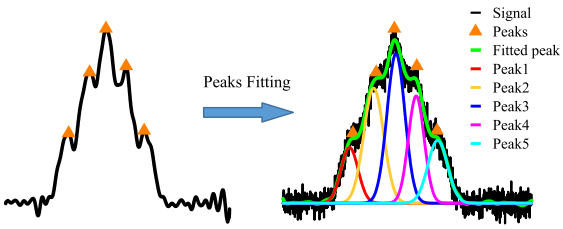


Fig. 3. Illustration of the peaks fitting process.

overlapping peak fitting algorithm. Specifically, the number of peaks is first determined based on the length of fp, and the coding length of the individual is further determined. Then, the boundary of the dimension in the individual corresponding to the position of the peaks is set based on the value of fp. Finally, the boundary of the dimension in the individual corresponding to the width of the peaks is set. In this work, the final fit is to the original signal, i.e., the signal that has not been smoothed and sharpened. After going through the smoothing, sharpening, and peak localization process, the resulting peak parameters are used for initialization of the peak fitting algorithm. Fig. 3 illustrates the process of peak fitting.

In this study, we define the grfe as follows:

$$\mathrm{grfe} = \left|(\mathrm{er}(\mathrm{iter}) - \mathrm{er}(\mathrm{iter}-1))\big/\mathrm{er}(\mathrm{iter})\right| \tag{11}$$

where grfe is the growth rate of fitting error, er is the fitting error, and iter indicates the current iteration. Specifically, the positions of all the fp under the current sc are used to initialize the PSO for an individual. Then, the signal is fit with the PSO algorithm and the fe is calculated. If grfe is less than the Th, it means that there are small false peaks under the current sc. According to the literature [32], for the peak fitting problem, more number of subpeaks leads to smaller fes. Thus, theoretically, a larger number of sub-peaks is better. However, the peaks found should be of practical significance. In this study, when an increase in the number of peaks leads to a decrease in the error of the current iteration and the growth rate of the error, gref, is less than the Th, it is considered that there are false small peaks in the found peaks. Therefore, the results of the previous iteration are more realistic, i.e., the results of the previous iteration are better. The peak fitting process ends when these results are obtained. Fig. 4 shows the flowchart of the proposed method.

### D. Computational Complexity

Let the signal length be $L$, and the number of individuals, dimension, and maximum number of iterations of the swarm intelligence algorithm be $N$, $D$, and $T$. From Fig. 4, the computational complexity of the peak analysis algorithms proposed in this study mainly depends on signal smoothing, sharpening with peak localization, and peak fitting. The computational complexity of signal smoothing is $O(L)$. The computational complexity of signal sharpening and peak localization is $O(L)$. Note that the computational complexity of the peak fitting process depends on the fitting algorithm used. The computational complexity of the peak fitting process

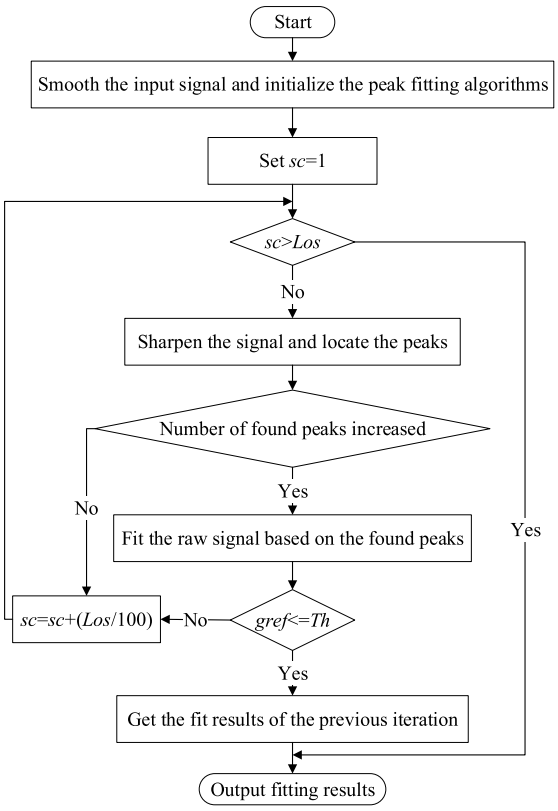


Fig. 4. Flowchart of the proposed algorithm.

using SLSMA1 is $O[D + T \times N(1 + \log N + D)]$. Therefore, the computational complexity of the proposed algorithm is $O\{L[D + T \times N(1 + \log N + D)]\}$. The run time of each step involved in the proposed method is discussed in Section IV-C.

## III. Experiment and Results

To analyze the accuracy of the different methods, this study compares three peak fitting methods: automatic methods, manual methods, and commonly used tools. The automatic method refers to the method proposed in this article that automatically obtains the peak parameters, identified by the abbreviation of the fitting algorithm plus the number 1, e.g., SLSMA1. The manual method is the one that requires the analyst to give the number of peaks, identified by the abbreviation of the fitting algorithm plus the number 2, e.g., SLSMA2. The commonly used peak fitting tools are identified by the name of the software, e.g., Origin and PeakFit. It should be noted that this section focuses on comparing the fitting accuracy of the automatic and manual methods. The comparison of the automatic methods with the commonly used peak fitting tools is given in Section IV-B.

### A. Data Acquisition

To verify the performance of the proposed method, two types of peak-shaped signals are used. The first type of signal is the synthetic peak, consisting of five gps superimposed at adjacent peak positions. With the in-built MATLAB function "AWGN," the SNR of the synthetic signal is set to 20, 21, and 22 dB, respectively, to simulate the ME signal. To construct

TABLE I
Peak Parameters of Synthetic Signals

| Parameter \ Peak | 1 | 2 | 3 | 4 | 5 |
|---|---|---|---|---|---|
| height | 1600 | 3000 | 4000 | 3000 | 1600 |
| position | 380 | 510 | 630 | 750 | 880 |

overlapping peaks, the parameters of the gps (i.e., height, width, and position) all usually need to be set to specific values. Inspired by Matsumura et al. [33] and Zhang et al. [34], the width of the gps in the synthetic signal is set to the same value in this study for the sake of brevity. Based on this, overlapping peaks are constructed by setting different heights or positions for the gps. The width of all gps is 120, and the other parameters of the synthetic signal are shown in Table I. The length of the synthetic signal is set to 1400 to demonstrate the baseline on both sides of the peaks. In addition, to further validate the proposed method on real-world signals, ME signals of three samples are collected. These samples are described in Table II. For Sample 1, the stock solutions are L-histidine (His), 2-(N-morpholino)-ethanesulfonic acid (MES), 18-Crown-6, and sodium hydroxide at concentrations (mM/L) of 40, 40, 20, and 150, respectively. The ME experimental setup of Sample 1 is consistent with those of the recently published works [7], [35]. From Table II, Sample 2 is a soybean seedling extract. It is selected from the whole soybean seedlings cultivated for 30 days, and the leaves are grounded and filtered, and the leaf juice is extracted as the sample to be measured. For Sample 2, the sample matrix solution in the sample to be tested is 2.5-mM MES/His 0.01-mM CTAB 5-mM 18-crown-6. For Sample 3, the ME experimental setup is consistent with those in [1]. For each sample in Table II, the ME injection and separation voltages were set to 500 and 1000 V, respectively. The frequency of both the excitation and reference signals of the ME detection system is 700 kHz, while the amplitudes are 5 and 20 $V_{pp}$, respectively. The final data acquisition was done by software written in MAX194 and LABVIEW. For Samples 1–3, the lengths of the acquired ME signals are 12 019, 18 001, and 27 501, respectively.

### B. Comparison of Signal Smoothing Methods

As mentioned in Section II-A, although the sharpening of peaks can improve the resolution of overlapping peaks, the signal is required to be relatively smooth to calculate the even-order derivatives. Therefore, it is important to choose a suitable signal-smoothing method. In the study, six commonly used signal smoothing methods are compared, including SG, Wl, Bw, CI, CII, and Et. The parameters of these filters were selected in an orthogonal experimental design. Depending on the characteristics of different filters, the orthogonal table was designed as a two-factor four level (for SG and Bw), a three-factor four level (for CI and CII), and a four-factor four level (for Et). Note that Wl depends on the order of the filter, and its value is set to a list of integers between 1 and 13.

TABLE II
DESCRIPTION OF DIFFERENT SAMPLES

| Sample | Description |
|---|---|
| 1 | 10 mM of $NH_4^+$, $K^+$, $Na^+$, $Ca^{2+}$, $Mg^{2+}$, and $Li^+$ chlorine salts mixture; running buffer is 20 mM MES/His, pH 6.0; The injection time is 14 seconds. |
| 2 | Soybean seedlings extract; running buffer is 20 mM MES/His 0.01 mM CTAB 10 mM 18-crown-6, pH 6.0; The injection time is 15 seconds. |
| 3 | Exosomes extract; running buffer is 40 mM MES/His, pH 7.0; The injection time is 40 seconds. |

TABLE III
PARAMETERS OF SIGNAL SMOOTHING METHODS

| Method / Parameter | SG | Wl | Bw | CI | CII | Et |
|---|---|---|---|---|---|---|
| order | 2 (2)* | 9 (6) | 4 (4) | 4 (1) | 4 (1) | 4 (1) |
| frame length | 105 (461) | | | | | |
| *ncf** | | | 0.012 | | | |
| *Rp** | | | | 0.1 (60) | | 0.1 (60) |
| *Rs** | | | | | 100 (70) | 100 (70) |
| *Wp** | | | | 0.012 (0.6) | | 0.012 (0.6) |
| *Ws** | | | | | 0.14 (0.9) | |

* The data outside the parentheses and inside the parentheses indicate the parameters for smoothing the synthetic and ME signals, respectively. *ncf* is the normalized cutoff frequency (π rad/sample), *Rp* is the decibels of peak-to-peak passband ripple (dB), *Rs* is decibels of stopband attenuation down from the peak passband value (dB), *Wp* is normalized passband edge frequency (π rad/sample), and *Ws* is normalized stopband edge frequency.

Experimentally, the parameters of each filter were selected as shown in Table III. The synthetic and ME signals have different lengths, and Table III gives a set of filter parameters for each of the two signals. The results of these methods are compared in terms of SNR, peak retention capability, and smoothness according to Section II-A.

Fig. 5 shows the comparison of the peak position retention capability of different signal smoothing methods. According to (4), the smaller the value of distance is the better the peak position retention capability of the smoothing methods. It can be seen that for both synthetic and ME signals, SG and Wl have better peak retention capability than other methods.

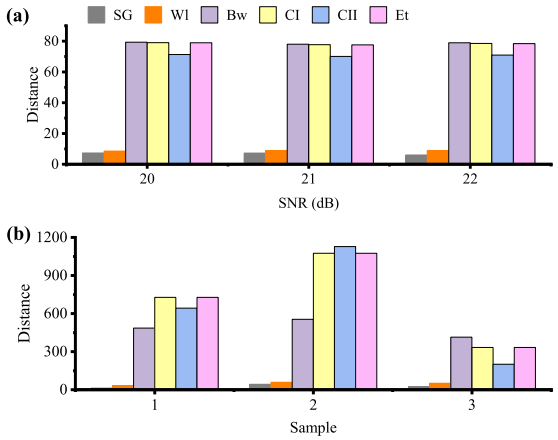


Fig. 5. Peak retention capability of different signal smoothing methods. (a) Synthetic signals. (b) ME signals. Distance is defined in (4). Each value is the average of 100 passes of signal smoothing.

TABLE IV
SMOOTHING RESULTS OF SG AND WL IN DB

| Signal / Filter | Sig1* | Sig2* | Sig3* | Sample1 | Sample2 | Sample3 |
|---|---|---|---|---|---|---|
| SG | 20.14 | 21.09 | 22.07 | 31.28 | 18.57 | 46.71 |
| Wl | 19.87 | 20.77 | 21.70 | 30.49 | 15.83 | 46.44 |

* Sig1, Sig2 and Sig3 denote synthetic signals with SNRs of 20 dB, 21 dB and 22 dB, respectively.

TABLE V
SMOOTHNESS OF WL RELATIVE TO SG

| Signal | Sig1 | Sig2 | Sig3 | Sample1 | Sample2 | Sample3 |
|---|---|---|---|---|---|---|
| Smoothness | 1.29 | 1.22 | 1.18 | 1.20 | 1.62 | 1.05 |

Signal smoothing methods should remove noise while retaining sufficient high-frequency information content of the signal. Therefore, SNR [as defined in (3)] is used to evaluate the performance of signal smoothing methods. Table IV shows the smoothing results in dB for filters SG and Wl. From Table IV, both SG and Wl can maintain the high-frequency information content of the signal. Overall, the results of SG are slightly better than those of Wl.

To further compare the signal smoothing performance of SG and Wl, the smoothness is also compared. Table V demonstrates the smoothness of Wl with respect to SG. From Table V, the smoothness of SG is slightly higher than that of Wl.

Fig. 6 shows the smoothing results of these methods for synthetic and ME signals of mixed chloride salt samples. From Fig. 6, all these methods can smooth the signals. However, only Wl and SG can maintain the peak positions before and after smoothing. Further comparison results of these two methods are shown in Fig. 7. As can be seen from Fig. 7, the SG filter exhibits good smoothing effects on the ME signals.

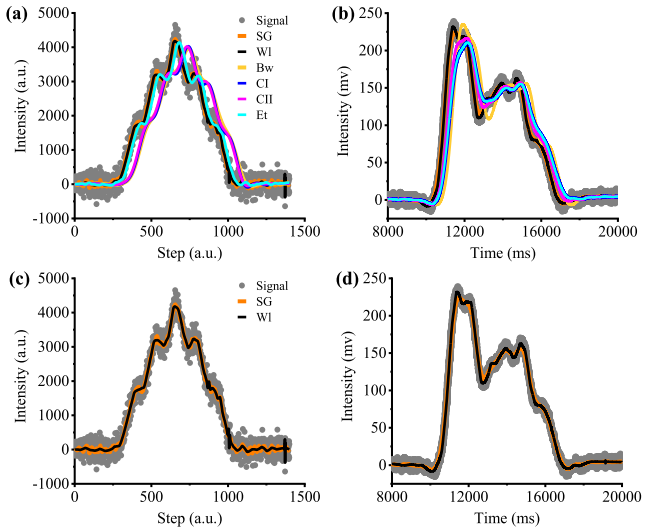


Fig. 6. Smoothing results of different signal smoothing methods. (a) and (c) Synthetic signal. (b) and (d) ME signal of mixed chloride salt sample.

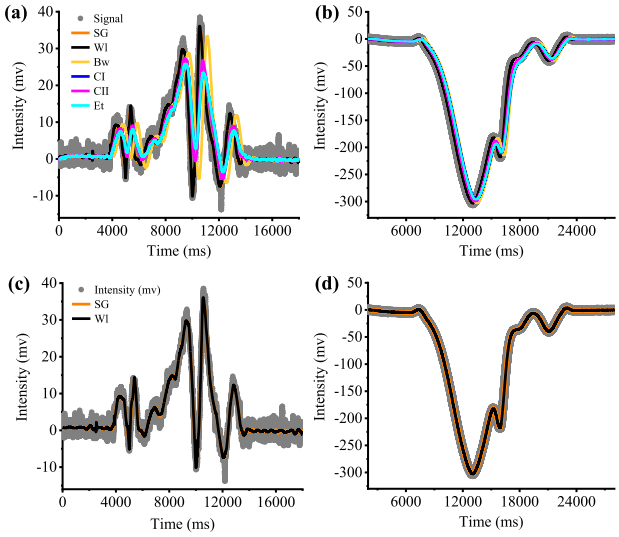


Fig. 7. Signal smoothing results of different signal smoothing methods. (a) and (c) ME signal of soybean seedling extract. (b) and (d) ME signal of exosome extract.

In summary, although the SG filter does not significantly outperform the other filters compared (e.g., the Wl filter) in smoothing the ME signals, the SG filter does show a certain degree of superiority in terms of the SNR, smoothness, and peak-position retention in terms of the overall smoothing effect. This may be related to the polynomial fitting [see (1)] and convolution properties [see (2)] of the SG filter. In addition, existing related studies [5], [36], [37] also illustrate the suitability of SG filters for the smoothing of electrophoresis signals. A discussion of the effect of the SG filter parameters will be given in Section IV-A.

### C. Results of Synthetic Signals

For synthetic signal, the sharpening results with different sc are illustrated in Fig. 8. From Fig. 8, the number of fp increases in a stepwise manner as sc increases. In addition,

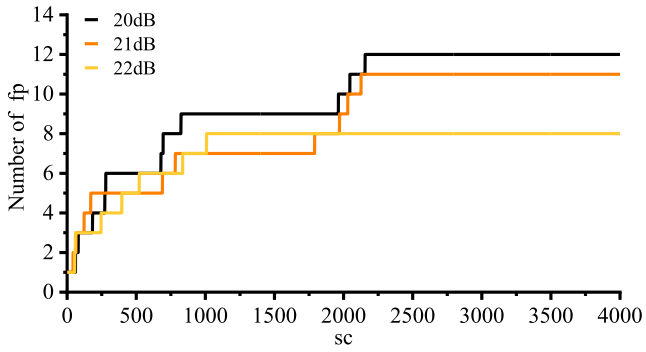


Fig. 8. Number of fp versus sc for the synthetic signals.

when sc is greater than the length of the synthetic signal (i.e., 1400), the number of fp is already significantly greater than the number of true peaks (i.e., 5). Thus, the search range of sc is between 1 and the length of the synthetic signals.

To demonstrate the effectiveness of the proposed peak sharpening method, the fitting performance of different algorithms is compared in this section. For the overlapping peak fitting problem, the fitting accuracy of the swarm intelligence algorithms (SLSMA [7], TWOA [8], and PSO [9]), the gradient algorithms (LM [10] and TRR [11]), and the simplex algorithm (NM [12]) are analyzed. Consistent with previous work [7], the population size and maximum number of iterations for the swarm intelligence algorithms in this study are set to 300 and 200, respectively. The other parameter settings of the swarm intelligence algorithms are shown in Table VI. In addition, the gradient algorithms (LM and TF) and the simplex algorithm (NM) are used via the nonlinear least squares solver "lsqnonlin" and the nonlinear programming solver "fminsearch" in MATLAB, respectively. Default parameters for these solvers are used. The parameters of these peak analysis algorithms are initialized by the proposed peaks sharpening method and the manual setting method, respectively. In contrast to the manual method, which requires empirical or visual determination of the number of peaks, the proposed sharpening method can automatically find peaks. To facilitate the description of different algorithms, the methods ending with the number 1 (e.g., SLSMA1) are based on the proposed sharpening method, and those ending with the number 2 (e.g., SLSMA2) are based on the manual method. According to (10), the individuals in the peak fitting process swarm intelligence algorithm are encoded as ($pos_1$, $wid_1$, $pos_2$, $wid_2$, . . . , $pos_n$, $wid_n$), i.e., a vector consisting of the position and width of the peaks, and the starting point of the gradient algorithm and the simplex algorithm is the position of the found peaks.

Fig. 9 shows the fes of different algorithms for the synthetic peaks. For the synthetic signal, the number of subpeaks is 5 (see Table I). When the number of fp after sharpening is 5, the average fes of different algorithms for the synthetic signal are shown in Fig. 9. For swarm intelligence algorithms, the fe of the proposed peaks sharpening method is smaller than that of the manual setting method. Fig. 9 also shows the comparison of the fes of the gradient algorithms and the

TABLE VI
PARAMETERS OF SWARM INTELLIGENCE ALGORITHMS

| Parameter | PSO* | TWOA* | SLSMA* |
|---|---|---|---|
| $c1$ | 2 | | |
| $c2$ | 2 | | |
| $w$ | decrease linearly from 0.9 to 0.4 | | |
| $\beta$ | | 1.5 | |
| $z$ | | | 0.03 |

* means the number 1 or 2, for example, PSO* is PSO1 or PSO2. $c1$ and $c2$ are the cognitive parameter and social parameter, respectively, $w$ is the inertia weight, $\beta$ is the Tent map parameter, and $z$ is Lévy flight parameter.

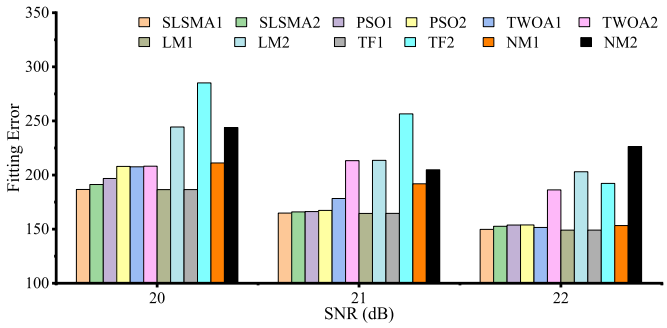


Fig. 9. fes of the synthetic signal. The fe is the mean of 100 fits of fe [as defined in (10)].

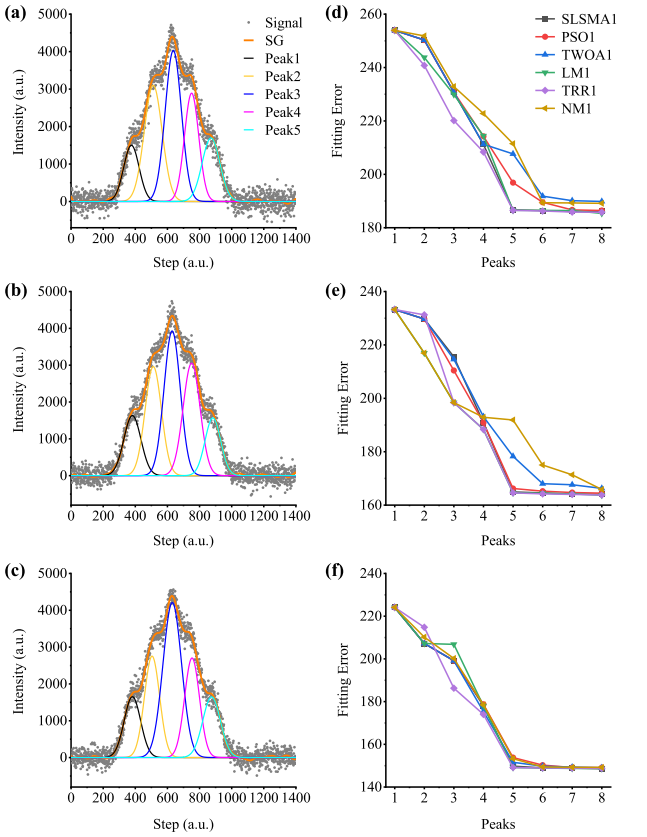


Fig. 10. Fitting results of the synthetic signals. The SNR of (a) and (d) is 20 dB, that of (b) and (e) is 21 dB, and that of (c) and (f) is 22 dB. The fe is the mean of 100 fits of fe [as defined in (10)].

simplex algorithm. For the gradient algorithms and the simplex algorithm, the fe based on the proposed overlapping peaks sharpening strategy is smaller. For the manual setting method, it is worth noting that the fes of the gradient algorithms and the simplex algorithm are slightly larger than those of swarm intelligence algorithms. In addition, the fe decreases overall with increasing SNR, except for the cases where the SNR is 21 dB (TWOA2) and the SNR is 22 dB (NM2).

When the number of fp after sharpening is 5, the fitting results of SLSMA1 for synthetic signals with different SNRs are shown in Fig. 10, where Fig. 10(a)–(c) correspond to 20, 21, and 22 dB, respectively. Due to the low resolution of the subpeaks of the synthetic signal, the number of fp for the overlapping peaks with different SNRs all start from 1. To analyze the effect of the number of fp on the fitting accuracy, the average fe at each number of fp is calculated. Fig. 10(d)–(f) shows the fes of the synthetic signals with different noise levels versus the number of fp. It can be seen that the error of the different algorithms decreases with the increase of the number of fp. In addition, for most algorithms, the fe decreases more quickly when the number of fp is less than 5. When the number of fp is greater than or equal to 5, the fe is almost constant. This trend is more obvious for synthetic signals with higher SNR, as shown in Fig. 10(f).

Table VII shows the average error between the peak positions of the fp and the true peak positions. For the five subpeaks in the synthetic signal, the position error of the third subpeak is smaller than that of the other subpeaks. It could be because the third subpeak is in the center and has the highest peak height. In addition, the overall small peak position errors in Table VII indicate that the proposed iterative overlapping peaks sharpening strategy is effective.

TABLE VII
PEAK POSITION ERRORS OF SYNTHETIC SIGNALS

| SNR \ Peak | 1 | 2 | 3 | 4 | 5 |
|---|---|---|---|---|---|
| 20dB | 11.8 | 9.9 | 2.5 | 10.8 | 10.7 |
| 21dB | 11.2 | 10.0 | 2.4 | 10.3 | 11.4 |
| 22dB | 10.9 | 10.5 | 2.0 | 10.7 | 10.4 |

### D. Results of ME Signals

In this section, the ME signals of different samples (see Table II) are analyzed, and the relationship between the number of fp and sc is shown in Fig. 11. As can be seen from Fig. 11, the number of fp shows a stepwise increase with the increase in the value of sc. This is consistent with the peak sharpening results of the synthetic signals (see Fig. 8). Thus, the iterative sharpening method proposed in this work is effective for the analysis of ME signals.

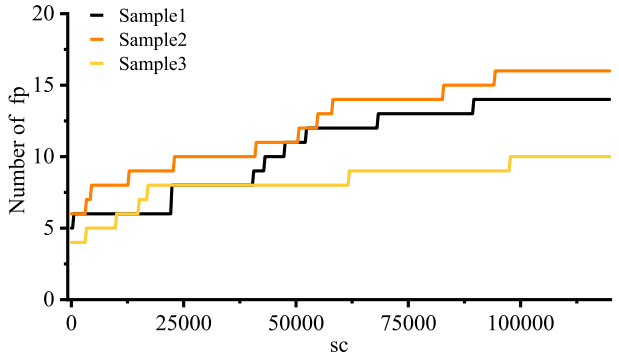


Fig. 11. Number of fp versus sc for the ME signals.

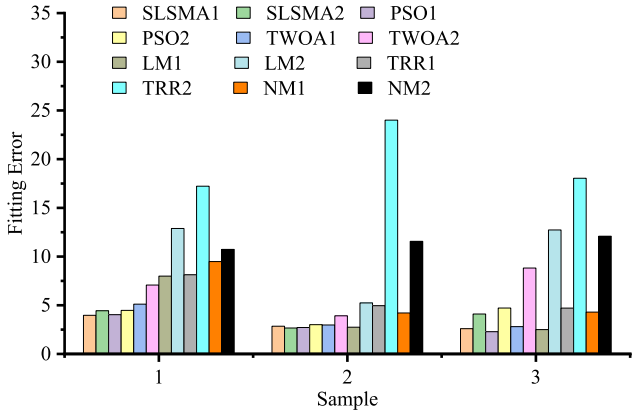


Fig. 12. fes of different algorithms. The fe is the mean of 100 fits of fe [as defined in (10)].

For Samples 1–3, the fes are shown in Fig. 12 when the number of fp is 6, 7, and 4, respectively. From Fig. 12, the fe of the proposed sharpening method is smaller than that of the manual method, which is consistent with the fitting results of the synthetic peaks (Fig. 9). In Fig. 12, for the swarm intelligence algorithms SLSMA, PSO, and TWOA, the ME signal fes after using the proposed peak sharpening strategy are reduced by 13.5%, 23.7%, and 40.0% on average, respectively.

Fig. 13 shows the fes of different algorithms for ME signals. Although the parameters of each subpeak in ME signals are unknown, the number of peaks can still be observed from the ME signals. The fe of ME signals versus the number of fp is shown in Fig. 13(b)–(d), respectively. Unlike the synthetic signals, the number of fp in the ME signals starts from 4, 6, and 3, respectively. For SLSMA1 and PSO1, the fe of Sample 1 decreases rapidly as the number of fp increases from 4 to 6; when the number of peaks continues to increase, the fe of these two algorithms remains almost constant. Note that although the error of the other algorithms decreases as the number of fp increases, a clear turning point (i.e., the number of fp is 6) is not observed. For Samples 2 and 3, similar results are presented. The results are consistent with the fitting results of the synthetic peaks (Fig. 10). Table VIII lists the comparison of the fes of the swarm intelligence algorithms. It can be seen that the PSO algorithm gives slightly better results than the other two algorithms. On the one hand, for the analysis of ME signals, a high stability of the peak fitting algorithm is required. On the other hand, although the fitting accuracy is improved with the help of the proposed sharpening strategy, the swarm intelligence algorithms used in this article are metaheuristic algorithms, the robustness still needs to be discussed, which will be given in Section IV-B.

TABLE VIII
FES OF SWARM INTELLIGENCE ALGORITHMS

| Sample \ Method | PSO1 | SLSMA1 | TWOA1 |
|---|---|---|---|
| 1 | **4.53** | 4.70 | 5.11 |
| 2 | 2.71 | 2.71 | 3.01 |
| 3 | **2.16** | 2.33 | 2.42 |

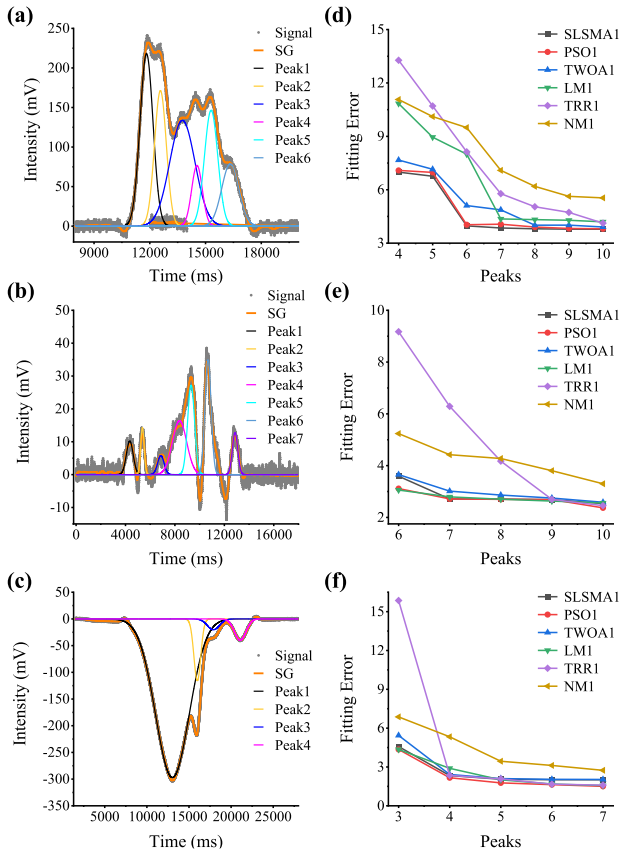


Fig. 13. Fitting results of the ME signals. (a) and (d) Sample 1, (b) and (e) Sample 2, and (c) and (f) Sample 3. The fe is the mean of 100 fits of fe [as defined in (10)].

From the above comparison of results, it can be seen that the proposed iterative peak sharpening strategy can improve the fitting accuracy of overlapping peaks. From Fig. 4, the advantage of the proposed method (e.g., SLSMA1) over existing similar methods (e.g., SLSMA2) is that the peak fitting parameters can be set automatically. Nevertheless, the computational complexity of the proposed method in this study is higher because it combines the even-order derivative sharpening process with the existing methods. Therefore, it is necessary to choose a suitable peak fitting method when analyzing ME signals from complex samples. The recommendation is to use

TABLE IX
PEAK FINDING RESULTS FOR DIFFERENT FRAME LENGTHS

| fp \ fl | 59 | 85 | 99 | 121 | 607 | 809 |
|---|---|---|---|---|---|---|
| 2 | ○ | ○ | ○ | ○ | ○ | ○ |
| 3 | ○ | ○ | ○ | ○ | ○ | ● |
| 4 | ○ | ○ | ○ | ○ | ● | ● |
| 5 | ○ | ○ | ○ | ● | ● | ● |
| 6 | ○ | ○ | ● | ● | ● | ● |
| 7 | ○ | ● | ● | ● | ● | ● |
| 8 | ○ | ○ | ● | ● | ● | ● |
| 9 | ● | ● | ○ | ● | ● | ● |
| 10 | ○ | ○ | ● | ● | ● | ● |

● and ○ denote presence and absence, respectively.

the manual method for the analysis of ME signals with a high number of subpeaks and a low SNR; otherwise, use the automatic method.

## IV. DISCUSSION

### A. Effect of Smoothing Parameters

As mentioned in Section III-B, the performance of signal smoothing methods affects the results of sharpening and peak localization. Therefore, it is necessary to discuss the effect of smoothing parameters on peak finding results. The parameters that affect the filtering effect in SG filters are polynomial order and frame length (fl). In addition, the number of smoothing also affects the smoothness of the filtered signal. The more the number of smoothing, the smoother the filtered signal is and the less the possibility of false peaks in the signal after sharpening using even order derivatives. In this section, both the polynomial order and the number of smoothing are set to 2. In this section, we focus on the relationship between the fl of the SG filter and the peak-finding results, as shown in Table IX. It can be seen that the larger fl is, the fewer the number of peaks found in the initial stage of peak finding. Combining the characteristics of ME signals with the principle of SG filter, the fl value in this study is chosen from an odd number between 121 and 809.

### B. Robustness

Swarm intelligence algorithms (SLSMA, PSO, and TWOA), all of which are metaheuristics, are involved in the peak fitting methods proposed in this study. There is some randomness in the computational results of these metaheuristic algorithms, which is a challenge for ME overlapping peak analysis algorithms that require high fitting accuracy. Although the effectiveness of the proposed algorithms has been tested using synthetic and ME signals in Sections III-C and III-D, further robustness analysis is still needed.

Fig. 14 shows the convergence curves of the proposed swarm intelligence-based overlapping peaks analysis algorithm. These convergence curves are derived from the fitting results of the ME signal. From Fig. 14, SLSMA1 can converge in about 120 iterations. In contrast, PSO1 converges more slowly. When fp = 6, i.e., the number of peaks found is 6, the final fe is also very close to that of fp > 6. At the maximum iteration, the fe of SLSMA1 is very close to that of PSO1 in most cases. Therefore, the swarm intelligence algorithm can be used for peak fitting with the assistance of the proposed peaks sharpening strategy.

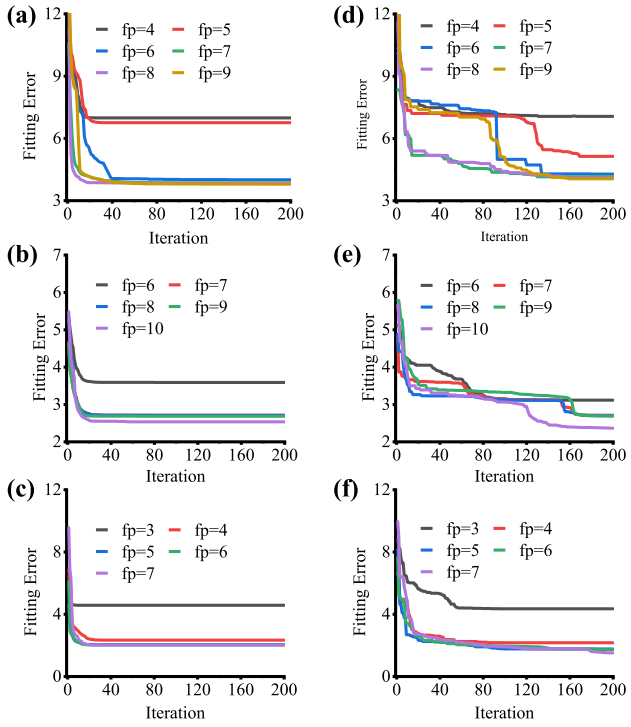


Fig. 14. Convergence curves of swarm intelligence-based peaks fitting algorithms for ME signals. SLSMA1 and PSO1 are shown in the left and right columns, respectively. The ME signals are the detection data for (a) and (d) Sample 1, (b) and (e) Sample 2, and (c) and (f) Sample 3, respectively.

To compare the proposed peak fitting methods with the commonly used peak fitting tools, the goodness of fit is defined as follows:

$$R^2 = 1 - \frac{\sum_{i=1}^{N} (y - y_{\text{fit}})^2}{\sum_{i=1}^{N} (y - \bar{y})^2} \tag{12}$$

where $R^2$ denotes the goodness of fit, $y$ denotes the original signal, $\bar{y}$ denotes the mean value of $y$, $y_{\text{fit}}$ denotes the fit signal, and $N$ denotes the number of data points in the signal.

Fig. 15 shows the fitting results of the proposed swarm intelligence-based overlapping peak analysis method and two commonly used peak analysis tools (PeakFit [38] and Origin [39]) for the ME signal. It can be seen that the goodness of fit of the proposed swarm intelligence-based peak fitting algorithm is slightly lower than that of the two tools. It should be noted that these tools are manual fitting methods, whereas the proposed method is more automated. Despite a certain degree of randomness in the swarm intelligence-based peak fitting algorithm, the results are close to those of the manual tools.

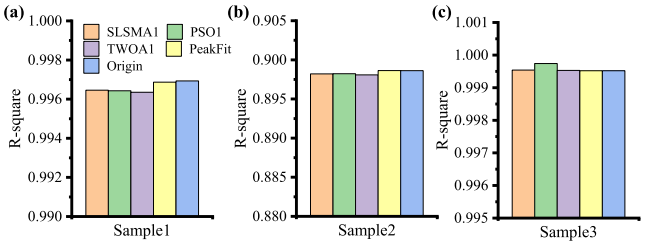


Fig. 15. Fitting results of ME signals for different peak analysis methods. (a)–(c) Samples 1–3, respectively. $R^2$ [as defined in (12)] is the average of 100 fits.

TABLE X
RUNNING TIME OF SIGNAL PREPROCESSING STEPS

| Time(s) / Sample | smoothing | sharpening | localization |
|---|---|---|---|
| 1 | 0.3528 | 0.0006 | 0.0158 |
| 2 | 0.1745 | 0.0007 | 0.0163 |
| 3 | 0.1064 | 0.0011 | 0.0277 |

Overall, for the peak fitting problem, the robustness of the swarm intelligence algorithms is reflected in the following aspects. First, the proposed peak fitting algorithm contains the steps of smoothing, sharpening and peak localization, and fitting, in which the smoothing algorithm selects the SG filter that can maintain the peak position, and the sharpening process iteratively improves the peak resolution, so the designed algorithm demonstrates certain robustness in principle. Second, the swarm intelligence algorithms can converge when fitting ME peaks (Fig. 14), indicating the robustness of the proposed algorithm. Finally, the comparison results with other state-of-the-art peak analysis methods (Fig. 15) also validate the robustness of the metaheuristic algorithms.

### C. Time Complexity Analysis

It is clear from Section II that the proposed peak analysis method involves the steps of smoothing, sharpening, peak finding, and fitting. Therefore, to analyze the computational complexity of the proposed method, it is necessary to analyze the run time of each step. For convenience, the steps prior to fitting are referred to as signal preprocessing steps. For ME signals, Table X shows the run time of the signal preprocessing steps. It can be seen that the sharpening step has the shortest running time. For the fitting step, the running times of the different algorithms were analyzed for Samples 1–3, when the number of peaks was 6, 7, and 4, respectively, according to Fig. 13. The run time of the fitting step is shown in Fig. 16. From Fig. 16, there is a small difference in the running time of different algorithms. This shows that the proposed sharpening method is effective.

### D. Summary

To analyze multiple subpeaks low-resolution overlapping peaks in ME signals, an iterative sharpening strategy is proposed in the study. To the best of authors' knowledge, the even-order derivative method is applied for the first time to the sharpening of ME signals. From the sharpening results of the synthetic signals (Fig. 8) and the ME signals (Fig. 11), it is clear that the number of fp increases stepwise with increasing sc. Nevertheless, it is still a challenge to choose the suitable sc value and to improve the final ME overlapping peaks fitting accuracy. This inspired the present study, i.e., an overlapping peaks analysis method based on an iterative sharpening strategy. The fitting results of the synthetic peaks (Figs. 9 and 10 and Table VII) and the ME peaks (Figs. 12–15 and Table VIII) show that the proposed method has a higher fitting accuracy compared to the manual method. This indicates that the proposed method is effective for overlapping peak analysis.

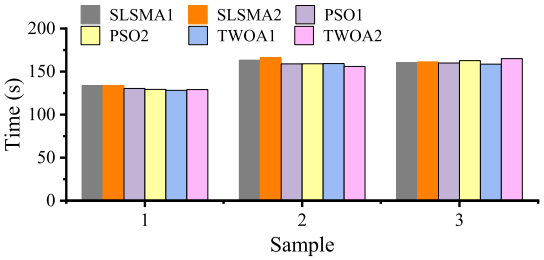


Fig. 16. Run time of the fitting step for ME signals. The value is the average of ten fits.

## V. CONCLUSION

To improve the fitting accuracy of ME signals containing overlapping peaks with low resolution and multiple subpeaks, a peak analysis method based on an iterative sharpening strategy is proposed in this work. The proposed method consists of three main steps: smoothing, sharpening and peak position localization, and fitting. First, the SG method is used in this study because it outperforms other commonly used signal smoothing methods in these metrics of peak retention ability, smoothness, and preservation of the high-frequency information content of the signal. Second, the smoothed signal is iteratively sharpened using the even-order derivative method, and then, the found peak parameters are used for the initialization of the overlapping peak fitting algorithms. Finally, the accuracy of the proposed method, the manual method, and the commonly used peak fitting tools are compared on the synthetic and ME signals. The results show that the proposed peak sharpening strategy can improve the accuracy of overlapping peak fitting. When fitting ME signals, the fitting accuracy of the proposed method is higher than that of the manual method and lower than that of the commonly used tools. This may be because the accuracy of peak position localization under the proposed peak sharpening strategy is slightly lower than that of the manual tools. Currently, the proposed overlapping peak analysis method is only applicable to ME signals, and its application needs to be extended in the future based on the characteristics of other types of detected signals.

## REFERENCES

[1] R. Sun, Y. Liu, H. Huang, H. Wang, L. Wang, and H. You, "Novel microchip electrophoresis–contactless conductivity method for detection and characterization of extracellular vesicles enriched for exosomes and microvesicles," *Bioanalysis*, vol. 14, no. 24, pp. 1547–1561, Dec. 2022.

[2] Y. Liu et al., "A pH-mediated field amplification sample stacking technique based on portable microchip electrophoresis heavy metal ion detection system," *Anal. Sci.*, vol. 39, no. 9, pp. 1475–1482, Sep. 2023.

[3] H. Alatawi et al., "Rapid determination of NSAIDs by capillary and microchip electrophoresis with capacitively coupled contactless conductivity detection in wastewater," *Electrophoresis*, vol. 43, no. 20, pp. 1944–1952, Oct. 2022.

[4] S. Mikkonen et al., "Capillary and microchip electrophoresis method development for amino acid monitoring during biopharmaceutical cultivation," *Biotechnol. J.*, vol. 17, no. 8, Aug. 2022.

[5] M. Masár et al., "Online coupling of microchip electrophoresis with ion mobility spectrometry for direct analysis of complex liquid samples," *Sens. Actuators B, Chem.*, vol. 302, Jan. 2020, Art. no. 127183.

[6] T. N. Samarasinghe, Y. Zeng, and C. K. Johnson, "Microchip electrophoresis assay for calmodulin binding proteins," *J. Separat. Sci.*, vol. 44, no. 4, pp. 895–902, Feb. 2021.

[7] W. He et al., "A novel unresolved peaks analysis algorithm for ME signal detection based on improved SMA," *IEEE Trans. Instrum. Meas.*, vol. 72, pp. 1–9, 2023.

[8] W. He et al., "A novel symmetrical peak fitting method based on improved WOA algorithm for the analysis of microchip electrophoresis signals," *Symmetry*, vol. 14, no. 12, p. 2603, Dec. 2022.

[9] N. A. Selamat, S. H. Md. Ali, K. N. B. Minhad, S. A. Ahmad, and J. Sampe, "A novel peak detection algorithm using particle swarm optimization for chew count estimation of a contactless chewing detection," *IEEE Trans. Instrum. Meas.*, vol. 71, pp. 1–12, 2022.

[10] R. Yang and Y. Zhang, "A method of low concentration methane measurement in tunable diode laser absorption spectroscopy and Levenberg–Marquardt algorithm," *Optik*, vol. 224, Dec. 2020, Art. no. 165657.

[11] P. Adrich and I. Zychor, "Least-squares fitting algorithm for peak pile-up correction in gamma-ray spectroscopy," *Nucl. Instrum. Methods Phys. Res. A, Accel. Spectrom. Detect. Assoc. Equip.*, vol. 990, Feb. 2021, Art. no. 164962.

[12] A. Mani-Varnosfaderani, M. J. Masroor, and Y. Yamini, "Evaluating different sparsity measures for resolving LC/GC-MS data in the context of multivariate curve resolution," *Chemometric Intell. Lab. Syst.*, vol. 200, May 2020, Art. no. 104004.

[13] Y. Li, C. Pan, Y. Xue, X. Meng, and Y. Ding, "A novel signal enhancement method for overlapped peaks with noise immunity," *Spectrosc. Lett.*, vol. 49, no. 4, pp. 285–293, Apr. 2016.

[14] M. F. Wahab, T. C. O'Haver, F. Gritti, G. Hellinghausen, and D. W. Armstrong, "Increasing chromatographic resolution of analytical signals using derivative enhancement approach," *Talanta*, vol. 192, pp. 492–499, Jan. 2019.

[15] J. Chen, C. Yang, H. Zhu, and Y. Li, "Adaptive signal enhancement for overlapped peaks based on weighting factor selection," *Spectrosc. Lett.*, vol. 52, no. 1, pp. 49–59, Jan. 2019.

[16] G. Hellinghausen, M. F. Wahab, and D. W. Armstrong, "Improving peak capacities over 100 in less than 60 seconds: Operating above normal peak capacity limits with signal processing," *Anal. Bioanal. Chem.*, vol. 412, no. 8, pp. 1925–1932, Mar. 2020.

[17] Y. Sun and J. Xin, "Lorentzian peak sharpening and sparse blind source separation for NMR spectroscopy," *Signal, Image Video Process.*, vol. 16, no. 3, pp. 633–641, Apr. 2022.

[18] C. Liang, C. Wang, X. Xue, X. Dou, and T. Chen, "Meter-scale and subsecond-resolution coherent Doppler wind LiDAR and hyperfine wind observation," *Opt. Lett.*, vol. 47, no. 13, p. 3179, 2022.

[19] M. Sadeghi, F. Behnia, and R. Amiri, "Window selection of the Savitzky–Golay filters for signal recovery from noisy measurements," *IEEE Trans. Instrum. Meas.*, vol. 69, no. 8, pp. 5418–5427, Aug. 2020.

[20] K. Hasan, S. T. Meraj, M. M. Othman, M. S. H. Lipu, M. A. Hannan, and K. M. Muttaqi, "Savitzky–Golay filter-based PLL: Modeling and performance validation," *IEEE Trans. Instrum. Meas.*, vol. 71, pp. 1–6, 2022.

[21] R. Janeliukstis, "Continuous wavelet transform-based method for enhancing estimation of wind turbine blade natural frequencies and damping for machine learning purposes," *Measurement*, vol. 172, Feb. 2021, Art. no. 108897.

[22] E. Balouji, O. Salor, and T. McKelvey, "Deep learning based predictive compensation of flicker, voltage dips, harmonics and interharmonics in electric arc furnaces," *IEEE Trans. Ind. Appl.*, vol. 58, no. 3, pp. 4214–4224, May 2022.

[23] Ö. Eris, S. Bulut Eris, C. Bilgin, and M. R. Bozkurt, "IIR based digital filter design for denoising the photoplethysmography signal," in *Proc. 29th Signal Process. Commun. Appl. Conf. (SIU)*, Jun. 2021, pp. 1–4.

[24] M. Nabian, Y. Yin, J. Wormwood, K. S. Quigley, L. F. Barrett, and S. Ostadabbas, "An open-source feature extraction tool for the analysis of peripheral physiological data," *IEEE J. Transl. Eng. Health Med.*, vol. 6, pp. 1–11, 2018.

[25] G. Wang, D. Li, L. Xing, S. Chang, S. Han, and H. Jiang, "A Hilbert and Gauss fitting peak searching algorithm combined with wavelet transform," in *Proc. 5th Int. Conf. Robot., Control Autom. Eng. (RCAE)*, Oct. 2022, pp. 75–79.

[26] S. Kumar and S. Sengupta, "Detection of peak wavelength of multi-FBG using higher-order derivative of wavelets multiresolution analysis and maximum likelihood estimation," *Opt. Commun.*, vol. 544, Oct. 2023, Art. no. 129621.

[27] A. Sadat and I. J. Joye, "Peak fitting applied to Fourier transform infrared and Raman spectroscopic analysis of proteins," *Appl. Sci.*, vol. 10, no. 17, p. 5918, Aug. 2020.

[28] H. Kalesse, T. Vogl, C. Paduraru, and E. Luke, "Development and validation of a supervised machine learning radar Doppler spectra peak-finding algorithm," *Atmos. Meas. Techn.*, vol. 12, no. 8, pp. 4591–4617, Aug. 2019.

[29] D. Liu, Y. Wang, C. Liu, K. Wang, X. Yuan, and C. Yang, "Blackout missing data recovery in industrial time series based on masked-former hierarchical imputation framework," *IEEE Trans. Autom. Sci. Eng.*, pp. 1–13, Jun. 2023.

[30] Y. Wang et al., "Multiscale feature fusion and semi-supervised temporal-spatial learning for performance monitoring in the flotation industrial process," *IEEE Trans. Cybern.*, vol. 54, no. 2, pp. 974–987, Feb. 2024.

[31] S. Yadav et al., "Evolutionary algorithm-based optimal wiener-adaptive filter design: An application on EEG noise mitigation," *IEEE Trans. Instrum. Meas.*, vol. 72, pp. 1–12, 2023.

[32] X. Lv, S. Wang, Y. Zhao, and P. Shan, "A reinforcement learning based method for protein's differential scanning calorimetry signal separation," *Measurement*, vol. 188, Jan. 2022, Art. no. 110391.

[33] T. Matsumura, N. Nagamura, S. Akaho, K. Nagata, and Y. Ando, "Spectrum adapted expectation-maximization algorithm for high-throughput peak shift analysis," *Sci. Technol. Adv. Mater.*, vol. 20, no. 1, pp. 733–745, Dec. 2019.

[34] Z. Zhang et al., "A combined deconvolution and Gaussian decomposition approach for overlapped peak position extraction from large-footprint satellite laser altimeter waveforms," *IEEE J. Sel. Topics Appl. Earth Observ. Remote Sens.*, vol. 13, pp. 2286–2303, 2020.

[35] J. Wang et al., "A novel planar grounded capacitively coupled contactless conductivity detector for microchip electrophoresis," *Micromachines*, vol. 13, no. 3, pp. 1–12, Feb. 2022.

[36] M. A. Wright, F. S. Ruggeri, K. L. Saar, P. K. Challa, J. L. P. Benesch, and T. P. J. Knowles, "Analysis of $\alpha$B-crystallin polydispersity in solution through native microfluidic electrophoresis," *Analyst*, vol. 144, no. 14, pp. 4413–4424, 2019.

[37] Y. Liu et al., "On-chip quantitative-PCR using integrated real-time detection by capillary electrophoresis," *Electrophoresis*, vol. 37, no. 3, pp. 545–552, Feb. 2016.

[38] M. F. Wahab and T. C. O'Haver, "Peak deconvolution with significant noise suppression and stability using a facile numerical approach in Fourier space," *Chemometric Intell. Lab. Syst.*, vol. 235, Apr. 2023, Art. no. 104759.

[39] P. Jusner et al., "Analyzing the effects of thermal stress on insulator papers by solid-state 13C NMR spectroscopy," *Cellulose*, vol. 29, no. 2, pp. 1081–1095, Jan. 2022.


**Wenhe He** received the M.S. degree from the School of Computer, Electronics and Information, Guangxi University, Nanning, China, in 2015, where he is currently pursuing the Ph.D. degree.

His main research interests include signal processing.

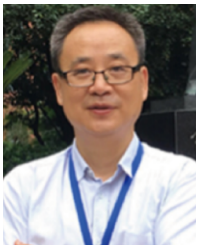

**Hui You** received the Ph.D. degree from the University of Science and Technology of China, Hefei, China, in 1999.

He is currently a Professor with the School of Mechanical Engineering, Guangxi University, Nanning, China. His research interests include microfluidics and biochips, MEMS, environmental monitoring devices, and ultrasonic cavitation and its applications.

**Zihao Lu** received the B.S. degree from Harbin Institute of Technology, Harbin, China, in 2019. He is currently pursuing the M.S. degree with Guangxi University, Nanning, China.

His research interests include microchip electrophoresis and ion detection.

**Yaping Liu** received the B.S. degree from Guangxi University, Nanning, China, in 2019, where he is currently pursuing the M.S. degree.

His research interests include microchip electrophoresis and ion detection

**Yuanfen Chen** received the Ph.D. degree from Iowa State University, IA, USA, in 2018.

She is currently an Associate Professor with the School of Mechanical Engineering, Guangxi University, Nanning, China. Her research interests include flexible electronics and printable electronics.

**Ying Liu** received the Ph.D. degree from Tongji University, Shanghai, China, in 2014.

She is currently an Associate Professor with the School of Civil Engineering and Architecture, Guangxi University, Nanning, China. Her current research interests include soil ontology theory.

**Cuimin Sun** received the Ph.D. degree from the University of Science and Technology of China, Hefei, China, in 2020.

She is currently an Associate Professor with the School of Computer, Electronics and Information, Guangxi University, Nanning, China. Her research interests include computer vision and pattern recognition.